

Communication

Localization error analysis for stereo X-ray image guidance with probability method

Hangyi Jiang^{a, e}, Wei R. Chen^{b, c}, Ge Wang^d, Hong Liu^{a, *}

^a Center for Bioengineering and School of Electrical and Computer Engineering, University of Oklahoma, Room 219, 202 West Boyd, Norman, OK 73019, USA

^b Department of Physics and Engineering, University of Central Oklahoma, Edmond, OK 73034, USA

^c Department of Physics and Astronomy, University of Oklahoma, Norman, OK 73019, USA

^d Department of Radiology, University of Iowa, Iowa 52242, USA

^e Department of Radiology, Johns Hopkins University, Baltimore, MD 21205, USA

Received 19 August 1999; received in revised form 8 May 2001; accepted 9 August 2001

Abstract

The mean value and standard deviation of localization error for the stereo imaging systems are derived based on probability theory. Compared with the maximum error analysis method used in our previous study, the new approach yields more informative and precise results as the guidance for X-ray imaging system design and protocol optimization. The prototype for our current study is a CCD based monoplane digital stereo X-ray imaging system. The imaging model consists of two X-ray sources and one detector plane. With perspective geometry, the least-square solution is derived to reconstruct 3-dimensional object points, such as a biopsy needle tip, from a pair of 2-dimensional digital radiographs. Under the conditions of our specific prototype, the measurement errors of interested points in the radiographs are modeled as random variables with Gaussian distribution. Such variables account for finite image system noise and positioning errors. Then, the 3D localization error, in terms of mean value and standard deviation, is formulated using measurement error, feature point location, and separation between the two X-ray sources and distance from source to detector. Both theoretical analysis and numerical simulation are performed. The mean value and standard deviation of the localization error are first evaluated using numerical simulation under practical imaging conditions. Then, the error estimates are given in simply analytic forms. Simulation and theoretical results are in excellent agreement. The results show that our prototype X-ray stereological imaging system is accurate and reliable to locate feature points in 3D for medical intervention. Imaging protocols can be effectively optimized through the 3D localization error analysis using the approximate formulas proposed in this study. © 2001 IPPEM. Published by Elsevier Science Ltd. All rights reserved.

Keywords: Stereotactic biopsy; Image guided therapy; Random error analysis; Stereo fluoroscopy

1. Introduction

With the advancement of computer science and digital technology, stereo image guidance has become an active area of investigation in radiological imaging. In clinical applications, digital stereotactic breast biopsy has been developed and successfully used for many years [1]. Similar technology and applications can also be found in stereo angiography, stereo image guided neurosurgery

and in other fields [2–4]. Compared with traditional planar radiology imaging, stereo technology can be used for 3D positioning of an interested object. Although the 3D information recovered from stereo image is limited compared with CT or MRI, it could provide us with sufficient clinical information for image guidance in various procedures. Additionally, with the advantages of low dose and high speed, this technique may lead to the development of a cost-effective, real-time stereo fluoroscopic image guidance system.

The stereo technology has been studied for decades [5–12]. One of the primary problems in stereo image guidance is the accuracy of the 3D localization, which is affected by stereo system errors and measurement errors. The

* Corresponding author. Tel.: +1-405-325-4286; fax: +1-405-325-7066.

E-mail address: liu@ou.edu (H. Liu).

measurement errors come from various sources, such as imaging noises, geometric distortions, and algorithm errors. These errors are unavoidable in practice and might be characterized as random variables with normal distribution. On the other hand, the stereo system errors, including parameter uncertainties of source–imager distance (SID), object–imager distance (OID) and separation distance between two X-ray sources, could be corrected by system calibration procedures.

In our previous work, we had proposed a 3D positioning error analysis method for stereo image guidance [13,14], with which the maximum value (or upper bound) of localization error had been derived. In practice, however, we noticed that the real values of the errors are usually much lower than the estimated upper bound. Therefore, a more precise error analysis method that gives us a better understanding of the positioning error is needed for the purpose of establishing guidelines for system design and protocol optimization. In practice, the mean value and standard deviation can provide us with more informative and precise characteristics of the positioning accuracy than the upper bound estimation. Our goal is to establish a relationship between the overall 3D errors and the standard deviations of the measurement errors. This study, using probability approach and treating the measuring errors as random variables, is an extension of our previous analysis using fixed maximum values. Compared with the maximum error analysis method, probability approach gives us more information on the characteristics of the 3D localization error by expressing it as mean value and stan-

dard deviation. In this report, the prototype stereo imaging system used for calculation and simulation consists of two X-ray sources and one CCD detector array. The measurement errors during 3D localization are described as random variables with Gaussian distribution. The 3D-localization error, in terms of mean value and standard deviation, is then formulated using measurement error, object location and system geometric parameters. A numerical integration formula is used as a gold standard in calculating the localization error. An approximation analytic formula, which is more convenient in practice, is derived based on the probability theory. Both theoretical analysis and numerical simulation are performed. The simulation results are in excellent agreement with the theoretical analysis. Our results show that our prototype X-ray stereological imaging system is accurate and reliable in locating interested points in three dimensions for medical intervention. Imaging protocols can be effectively optimized using the 3D localization error formulas derived in this paper.

2. Materials and methods

2.1. Least-square algorithm for 3D localization with stereo-images

Consider an elementary stereo X-ray imaging system shown in Fig. 1. Two X-ray sources are placed with a separation b . The origin of the reference coordinate system is set as the center between the two X-ray sources. The x -axis of the reference system is taken as the line connecting the two X-ray tubes. The imaging plane is coordinated by (u,v) . The u - and v -axes are parallel to the x - and y -axes, respectively. Its distance to the X-ray sources is f . The origin of the image plane is the perpendicular projection point of reference origin. To simplify the analysis, the scales of both coordinate systems are set to be the same. The position of the X-ray tubes with respect to the reference system are $T_1(-b/2,0,0)$ and $T_2(b/2,0,0)$, respectively. The object point $Q(x,y,z)$ in 3D space, projected onto the image plane, results in feature points $P_1(u_1,v_1)$ and $P_2(u_2,v_2)$ on each of the stereo-pair images.

There are many ways to recover the 3D point $Q(x,y,z)$ from its projections [5–7]. One of the direct ways is to reconstruct the 3D point from its projections by analytic geometric method [15]. With the registration of image points, $P_1(u_1,v_1)$ and $P_2(u_2,v_2)$ the object point $Q(x,y,z)$ can be resolved by the intersection of two straight lines which are specified by X-ray tubes and object's projections on the imaging plane.

The relationship between the 3D point $Q(x,y,z)$ and its projections P_i with respect to X-ray tube T_i is given by the following straight line equations:

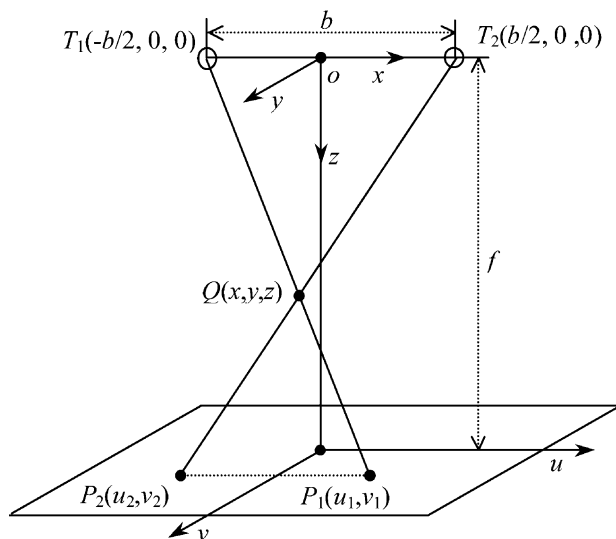


Fig. 1. The geometry of the elementary stereo X-ray imaging system. The separation between the two X-ray tubes is denoted as b and the origin of the reference system o - xyz is taken as the center of the base line. The image plane (u - v plane) is aligned with x - y plane. The z -axis points to the image plane. The source–image receptor distance is f . The 3D object point $Q(x,y,z)$ with respect to the world coordinate system is projected onto the u - v plane, with projection points $P_1(u_1,v_1)$ and $P_2(u_2,v_2)$ respectively.

$$\frac{x-x_{T_i}}{x_{P_i}-x_{T_i}} = \frac{y-y_{T_i}}{y_{P_i}-y_{T_i}} = \frac{z-z_{T_i}}{z_{P_i}-z_{T_i}} \quad (1)$$

Substituting the coordinates of $T_1, T_2, P_1,$ and P_2 into above equations yields two set of line equations, which can be expressed in matrix form as $\mathbf{AX}=\mathbf{B}$:

$$\begin{bmatrix} f & 0 & -(u_1+b/2) \\ 0 & f & -v_1 \\ f & 0 & -(u_2-b/2) \\ 0 & f & -v_2 \end{bmatrix} \begin{bmatrix} x \\ y \\ z \end{bmatrix} = \begin{bmatrix} -bf/2 \\ 0 \\ bf/2 \\ 0 \end{bmatrix} \quad (2)$$

This matrix equation represents a system of four equations with three unknowns (x,y,z) and thus, the solutions can be found using generalized inverse [16,17]. The solution of this equation can be derived as [14]:

$$\begin{bmatrix} x \\ y \\ z \end{bmatrix} = \frac{b \cdot [(u_1-u_2)-b]}{[(u_1-u_2)+b]^2+(v_1-v_2)^2} \begin{bmatrix} (u_1+u_2)/2 \\ (v_1+v_2)/2 \\ f \end{bmatrix} \quad (3)$$

2.2. Localization error analysis

Ideally, the coordinates of the 3D object can be accurately determined from its 2D projections (feature points) on the stereo image pairs according to Eq. (3) in the least-squares method. However, the impact on the 3D positioning, due to the unavoidable measurement errors in feature point identification, must be considered. These errors may come from various random noises, imaging geometric distortions, misidentification of feature points and other uncertainties. If we express the 3D coordinate error as a column vector $\Delta\mathbf{X}=[\Delta x, \Delta y, \Delta z]^t$, where $\Delta x, \Delta y,$ and Δz are the x, y and z error components of the object. Then the total 3D localization error can be expressed as:

$$\Delta r = \|\Delta\mathbf{X}\| = \sqrt{\Delta x^2 + \Delta y^2 + \Delta z^2} \quad (4)$$

Our purpose is to estimate the mean value and the variance of the random variable Δr .

Let $\Delta\mathbf{U}=[\Delta u_1, \Delta u_2, \Delta v_1, \Delta v_2]^t$ be measurement error vector, where $\Delta u_1, \Delta u_2, \Delta v_1$ and Δv_2 are errors of u_1, u_2, v_1 and $v_2,$ respectively. From Eq. (3), the calculated error $\Delta\mathbf{X}$ of the 3D object can be derived as [15]:

$$\Delta\mathbf{X} = \mathbf{P} \cdot \Delta\mathbf{U} \quad (5)$$

where,

$$\mathbf{P} = \begin{bmatrix} \frac{\partial x}{\partial u_1} & \frac{\partial x}{\partial u_2} & \frac{\partial x}{\partial v_1} & \frac{\partial x}{\partial v_2} \\ \frac{\partial y}{\partial u_1} & \frac{\partial y}{\partial u_2} & \frac{\partial y}{\partial v_1} & \frac{\partial y}{\partial v_2} \\ \frac{\partial z}{\partial u_1} & \frac{\partial z}{\partial u_2} & \frac{\partial z}{\partial v_1} & \frac{\partial z}{\partial v_2} \end{bmatrix}$$

In clinical applications, the measurement error $\Delta\mathbf{U}$ can be regarded as a random vector with normal distribution. This assumption is acceptable for the reason that the error may be caused by various uncertainties that can be described as independent random variables. According to the central limit theorem, the distribution of the sum of independent random variables approaches a normal distribution. Therefore, the calculated 3D coordinate error $\Delta\mathbf{X}$ can also be treated as normally distributed random vector with a zero mean value since they are linear combination of the measuring errors. The joint probability density function of random variables ($\Delta x, \Delta y, \Delta z$) can be expressed as [15–19]:

$$f(\Delta\mathbf{X}) = \frac{1}{\sqrt{(2\pi)^3(\det\mathbf{C})}} \exp\left\{-\frac{1}{2}(\Delta\mathbf{X})\mathbf{C}(\Delta\mathbf{X})^t\right\} \quad (6)$$

where, $\mathbf{C} = \begin{bmatrix} \sigma_x^2 & \gamma_{xy} & \gamma_{xz} \\ \gamma_{xy} & \sigma_y^2 & \gamma_{yz} \\ \gamma_{xz} & \gamma_{yz} & \sigma_z^2 \end{bmatrix}$ is the covariance matrix and

$\det\mathbf{C}$ is the determinant of \mathbf{C} . The terms $\sigma_x^2, \sigma_y^2,$ and σ_z^2 are the variances of random variables $\Delta x, \Delta y,$ and $\Delta z;$ and γ_{xy}, γ_{xz} and γ_{yz} are the covariances between the $\Delta x\Delta y, \Delta x\Delta z,$ and $\Delta y\Delta z$ channels, respectively. The mean value (μ_r) and variance (σ_r) of the random variable $\Delta r,$ which is 3D localization error defined by Eq. (4), are given by [19]:

$$\begin{cases} \mu_r = E(\Delta r) = \int \int \int_{V(\infty)} \Delta r f(\xi, \eta, \zeta) d\xi d\eta d\zeta \\ \sigma_r = D(\Delta r) = \sqrt{\int \int \int_{V(\infty)} \Delta r^2 f(\xi, \eta, \zeta) d\xi d\eta d\zeta - \mu_r^2} \end{cases} \quad (7)$$

where, $\Delta r = \sqrt{\xi^2 + \eta^2 + \zeta^2}, (\xi, \eta, \zeta)$ are the integration variables and $V(\infty)$ is the volume of integration sphere: $\xi^2 + \eta^2 + \zeta^2 < \infty.$

No analytic solutions are possible to obtain μ_r and variance σ_r using Eq. (7). Numerical integration must be carried out in this case [18]. To perform the numerical integration, we must determine the covariance matrix \mathbf{C} . From Eq. (5), with Gauss’s law of propagation of errors

[14], the terms of matrix **C** can be derived as (see Appendix A):

$$\begin{cases} \sigma_x^2 \approx \left(2x^2 + \frac{b^2}{2}\right) \cdot \frac{z^2 \sigma_m^2}{b^2 f^2} \\ \sigma_y^2 \approx \left(2y^2 + \frac{b^2}{2}\right) \cdot \frac{z^2 \sigma_m^2}{b^2 f^2} \\ \sigma_z^2 \approx 2z^2 \cdot \frac{z^2 \sigma_m^2}{b^2 f^2} \end{cases} \quad (8)$$

and

$$\begin{cases} \gamma_{xy} \approx 2xy \cdot \frac{z^2 \sigma_m^2}{b^2 f^2} \\ \gamma_{xz} \approx 2xz \cdot \frac{z^2 \sigma_m^2}{b^2 f^2} \\ \gamma_{yz} \approx 2yz \cdot \frac{z^2 \sigma_m^2}{b^2 f^2} \end{cases} \quad (9)$$

In Eqs. (8) and (9), σ_m^2 is the variance of random measuring errors, (x, y, z) are the coordinates of the 3D point (see Fig. 1), and f and b are geometric parameters of the stereo X-ray system. Since the density function of the random localization error is related to these parameters, we can conclude that the mean value and the variance of 3D localization error are governed by both 3D point location and the stereo system parameters. Numerical results with respect to the 3D point locations or system parameters will be given in Section 2.3.

We now give an approximation of the mean and variance of 3D localization error in analytic forms that are more convenient in system design. With Eq. (5), we know that Δx , Δy and Δz are normally distributed with zero mean values, If they were independent with equal variance σ^2 , Δr would be a random variable with Maxwell distribution and its mean value and standard deviation could be immediately obtained [19]. In practice the x and y coordinates of the object are very small since the object of interest is usually positioned at the center of the view field (see Fig. 1). With Eq. (9), the covariance γ_{xy} , γ_{xz} and γ_{yz} are close to zero in this case. In other words, it is reasonable to assume that Δx , Δy and Δz are independent. Furthermore, from Eq. (8) we can conclude that both σ_x^2 and σ_y^2 are less than σ_z^2 . Assuming that Δx , Δy and Δz are with equal variance σ^2 , we obtain an approximation of the 3D localization error in analytic form with the Maxwell distribution:

$$\begin{cases} \mu_r \leq S'_\mu 2\sqrt{(2/\pi)}\sigma_z = \frac{S_\mu z^2 \sigma_m}{bf} \\ \sigma_r \leq S'_\sigma \sigma \sqrt{\left(3 - \frac{8}{\pi}\right)}\sigma_z = \frac{S_\sigma z^2 \sigma_m}{bf} \end{cases} \quad (10)$$

where, S_μ and S_σ are numerical coefficients. They can

be determined based on the numerical integration of Eq. (7):

$$\begin{cases} S_\mu \geq \frac{bf}{z^2 \sigma_m} E(\Delta r) \\ S_\sigma \geq \frac{bf}{z^2 \sigma_m} D(\Delta r) \end{cases} \quad (11)$$

Let $K = \frac{f}{z}$ denote the magnification factor of the X-ray

imaging system [20], and $\tan \theta = \frac{(b/2)}{z}$ indicates the tangent of view angle of the object with X-ray tubes (see Fig. 2). Then the estimation formula of the 3D localization error can be rewritten as:

$$\begin{cases} \mu_r \leq \frac{S_\mu \sigma_m}{2 \cdot K \cdot \tan \theta} \\ \sigma_r \leq \frac{S_\sigma \sigma_m}{2 \cdot K \cdot \tan \theta} \end{cases} \quad (12)$$

This result clearly shows that the mean value and the standard deviation of 3D localization error are both inversely proportional to the magnification factor of the X-ray system, and to the object view angle. They are also both proportional to the variance of measuring errors as expected.

2.3. Numerical integration and computer simulation

Numerical integration was performed according to Eq. (7) in order to establish the relationship between the overall 3D localization error and various factors that affect the 3D positioning accuracy. In performing the numerical integration, the standard deviation of random measuring error (σ_m) was assumed to be unity, so that the calculated results can be regarded as the ratio of the overall 3D localization error to the measuring errors. To verify the theoretical analysis results, a computer simulation was performed. Given system parameters and an object point in 3D space, the ideal projections (u_1, v_1) and (u_2, v_2) in the stereo pairs were calculated according to the perspective projection model of the stereo system [7]. Then, a normally distributed random noise with zero mean value was added to the ideal projection data to simulate measuring errors. Afterwards, the object coordinate was reconstructed from these noisy data with the least-square solution specified by Eq. (3). The resultant 3D localization error was calculated according to the definition given by Eq. (4). This procedure was performed 100 times for each given object point to ensure statistical significance. Then the mean value and the standard deviation of the 3D localization error were calculated to compare with the theoretical analysis results.

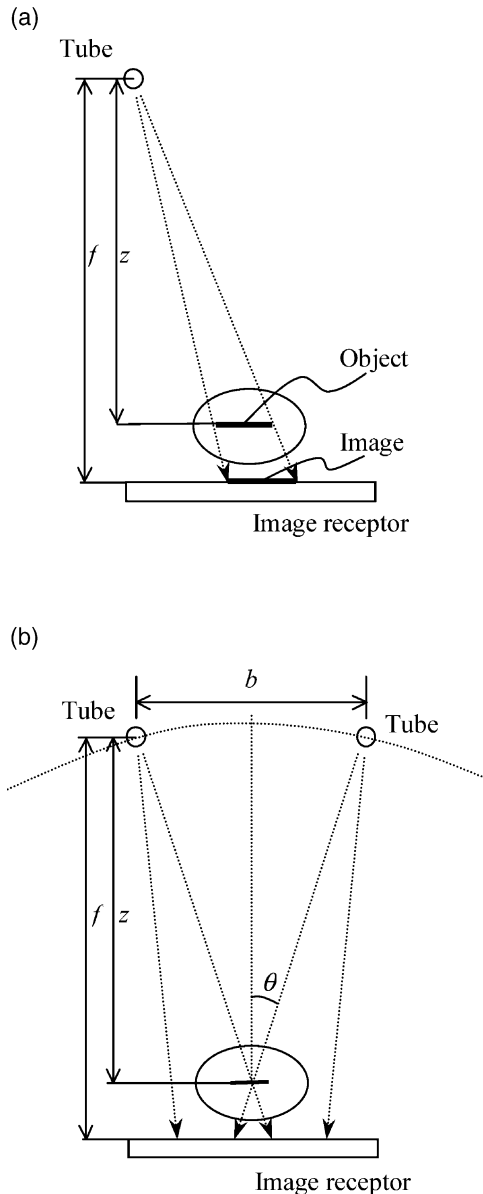


Fig. 2. Illustration (a) shows the magnification factor that is the ratio of image size to object size. It can be determined by the ratio of the altitude of the two triangles, i.e. (f/z) . The mean of the object view angle θ is given in (b); the view angle increases as the object moves closer to the X-ray tubes and the 3D localization error decreases as indicated by Eq. (12).

3. Results

Numerical analysis results of the 3D localization error, determined by numerical integration according to Eq. (7), are presented in Figs. 3 and 4.

Fig. 3 illustrates the effects of the stereo geometric parameters, f and b , on 3D localization error, by fixing the object point as $(x,y,z)=(50, 50, 490)$ mm. We let f vary from 500 to 800 mm, and b from 200 to 500 mm. As expected, both the mean value and standard deviation of the 3D localization error are inversely proportional

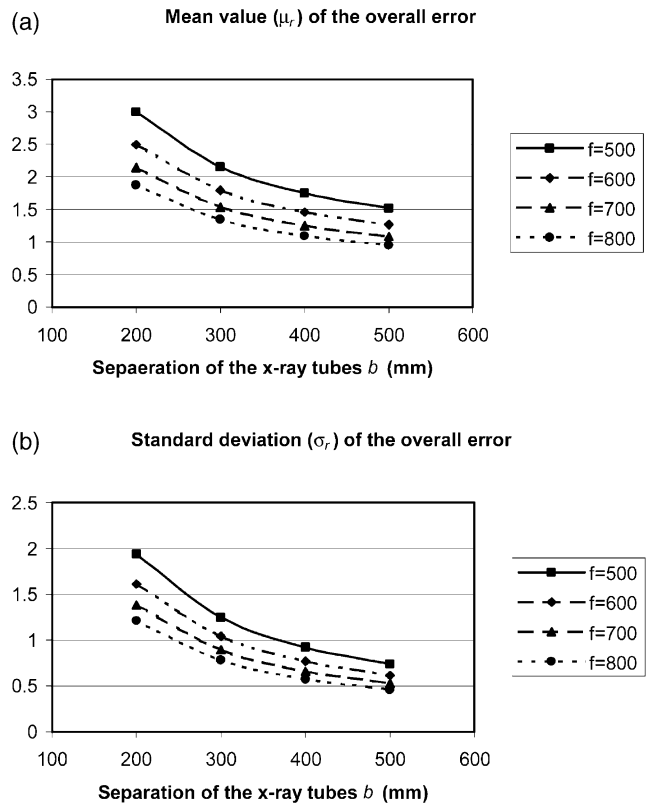


Fig. 3. Localization errors determined by numerical integration using Eq. (7). The object point coordinate was fixed in the position $(x,y,z)=(50, 50, 490)$ mm and the system geometric parameters f and b varied to illustrate their effects on 3D localization error. Both the mean value (a) and standard deviation (b) of the errors are inversely proportional to the system parameters, f and b .

to the parameters f and b if the object position remains unchanged (see Eq. (10)). Because the z component of the object coordinate was kept constant, the increases of f and b led to the increases of magnification factor (K) of the X-ray imaging system and the view angle (θ) of the object with the X-ray tubes. As Eq. (12) pointed out, the 3D localization error decreases with the increases of K and θ .

Fig. 4 shows the relationship between the 3D localization accuracy and the object position in x - y plane while the system geometric parameters and the depth z of the object position are fixed. In this case, the magnification factor of the imaging system remains constant, and the object view angle varies slightly with the x - y coordinates shifting within a limited area (see Fig. 2). The effect of x , and y components of the object position on the 3D localization error is smaller than other factors. The resultant values show that the impact of x , and y components of object position on the 3D localization error is smaller than other factors—both the mean value and the standard deviation of the error had only minor changes. In fact, from Eq. (8), we can see that the variance of Δx and Δy are much smaller than the variance of Δz , so that the 3D localization error is mainly governed by the depth

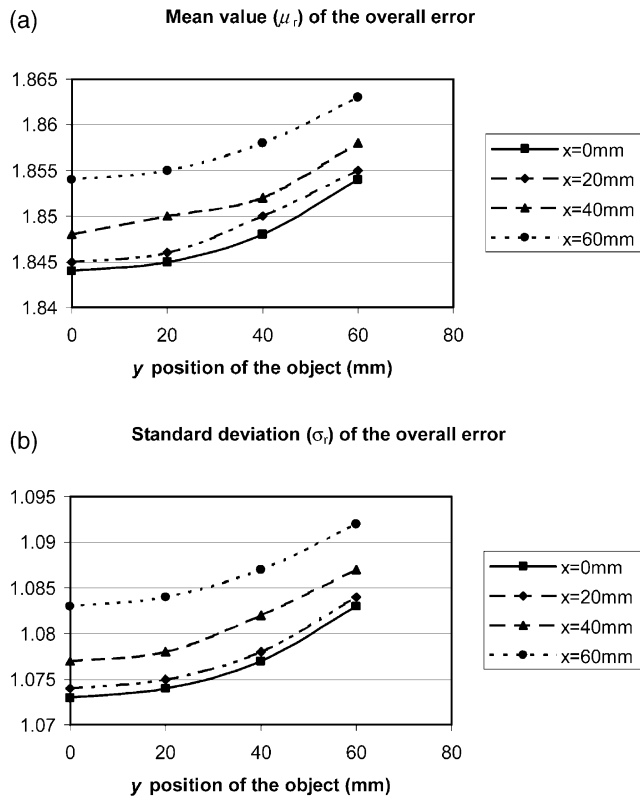


Fig. 4. Mean value (a) and standard deviation (b) of the localization errors determined by numerical integration using Eq. (7). The system geometric parameters f , b and object point depth z were fixed as ($f=600$ mm, $b=300$ mm, $z=500$ mm) and the x and y components of the object position varied to illustrate their effects on the 3D localization error.

z of the object position, if the system geometric parameters remain unchanged. Furthermore, the impact of the x and y components on the total error is symmetric.

To verify the results of above analysis, a computer simulation was performed and the results are presented in Figs. 5 and 6. Comparing with the curves in Figs. 3 and 4, the results from computer simulation are in excellent agreement with that of numerical integration.

In Section 2.2, we also derived analytic formula (Eq. (10)) to approximate 3D localization error. In this equation, experimental constants S_μ and S_σ are used to modify the estimation result for better agreement with the theoretical predication. They can be determined based on the numerical integration. In our case, S_μ and S_σ are calculated and presented in Tables 1 and 2, respectively. For our specific CCD based digital stereo prototype [13,14], S_μ and S_σ were chosen as 1.58 and 0.82 respectively. We then have:

$$\begin{cases} \mu_r \leq \frac{1.58 \times z^2}{bf} \sigma_m \\ \sigma_r \leq \frac{0.82 \times z^2}{bf} \sigma_m \end{cases}$$

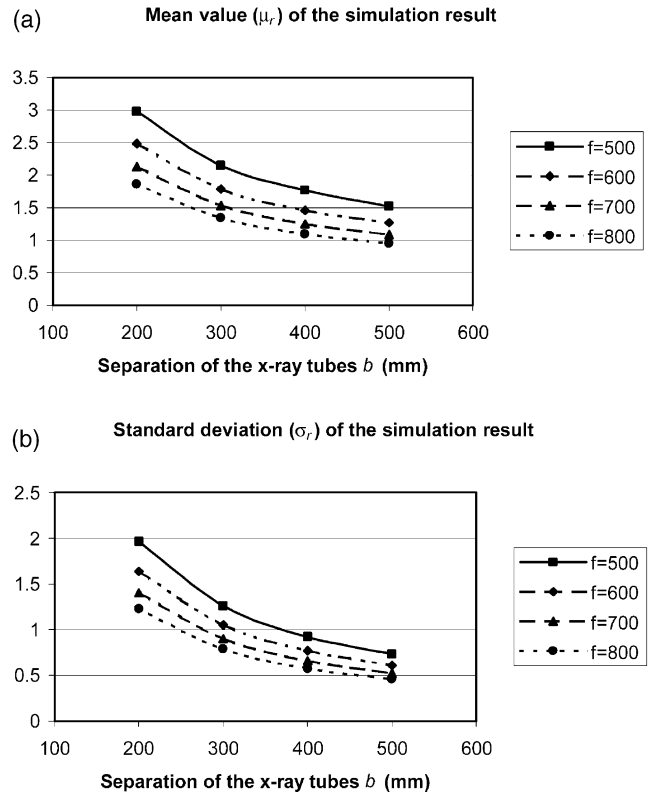


Fig. 5. Simulation results in comparison with the theoretical result in Fig. 3. The object point coordinate was fixed as: $(x,y,z)=(50, 50, 490)$ mm and the system geometric parameters, f and b , were varied.

As an example, estimation results are given in Fig. 7, in comparison with the theoretical analysis. Fig. 7 shows that the result from approximation equation is consistent with the expected value.

4. Discussion and conclusion

In practice, it is reasonable to regard the measuring errors as random variables of normal distribution with zero means, because the errors may be produced by various uncertainties which can be described as independent random variables. According to the central limit theorem, under certain conditions, the distribution of the sum of independent random variables approaches a normal distribution.

In this paper, the error of 3D point localization was analyzed with the probability approach. We derived a closed form solution for reconstructing a 3D point using the least-square method. Based on the least-squares solution and with the error propagation law, the 3D localization error was analyzed in terms of the object location, the measurement error, the separation between the two X-ray sources, and the distance from the source to the detector. The mean value and standard deviation of localization error were expressed by a numerical inte-

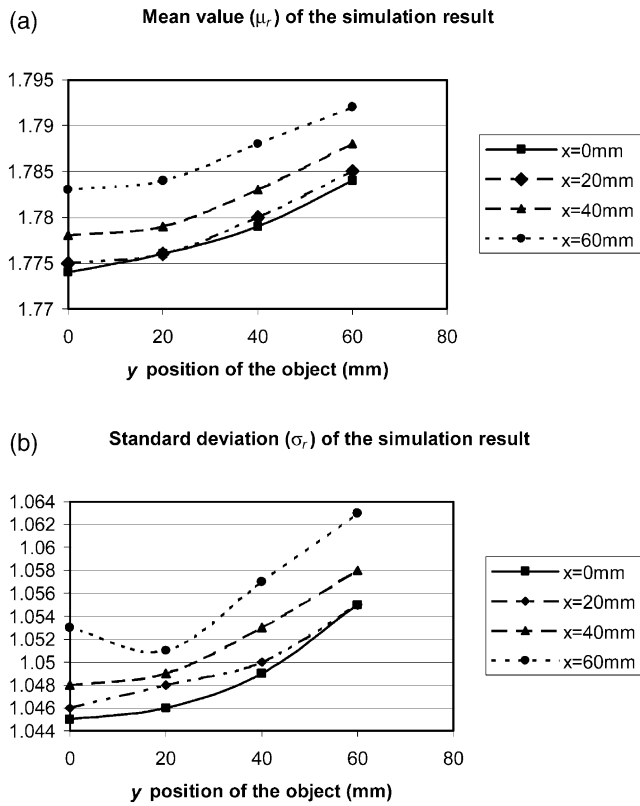


Fig. 6. Simulation results in comparison with the theoretical result in Fig. 4. The system geometric parameters f , b and object point depth z were kept as ($f=600$ mm, $b=300$ mm, $z=500$ mm) and the x and y components of the object position were varied.

Table 1

Calculated numerical coefficients S_μ and S_σ according to Eq. (11) and the theoretical results (Fig. 3). In this case, the object point coordinate was fixed in the following position: $(x,y,z)=(50, 50, 490)$ mm. The system geometric parameters were varied

	S_μ				S_σ			
	$b=200$ mm	$b=300$ mm	$b=400$ mm	$b=500$ mm	$b=200$ mm	$b=300$ mm	$b=400$ mm	$b=500$ mm
$f=500$ mm	1.248	1.345	1.456	1.578	0.807	0.781	0.768	0.769
$f=600$ mm	1.248	1.345	1.456	1.578	0.807	0.781	0.768	0.769
$f=700$ mm	1.248	1.345	1.456	1.578	0.807	0.781	0.768	0.769
$f=800$ mm	1.248	1.345	1.456	1.578	0.807	0.781	0.768	0.769

Table 2

Experimental constants S_μ and S_σ determined by the Eq. (11) and the theoretical results (Fig. 4). The system geometric parameters f , b and object point depth z were kept as ($f=600$ mm, $b=300$ mm, $z=500$ mm). The x and y components of the object position were varied

	S_μ				S_σ			
	$y=0$ mm	$y=20$ mm	$y=40$ mm	$y=60$ mm	$y=0$ mm	$y=20$ mm	$y=40$ mm	$y=60$ mm
$x=0$ mm	1.327	1.328	1.330	1.335	0.772	0.773	0.775	0.779
$x=20$ mm	1.328	1.329	1.331	1.336	0.773	0.774	0.776	0.780
$x=40$ mm	1.330	1.331	1.334	1.338	0.775	0.776	0.779	0.783
$x=60$ mm	1.335	1.336	1.338	1.343	0.779	0.780	0.783	0.786

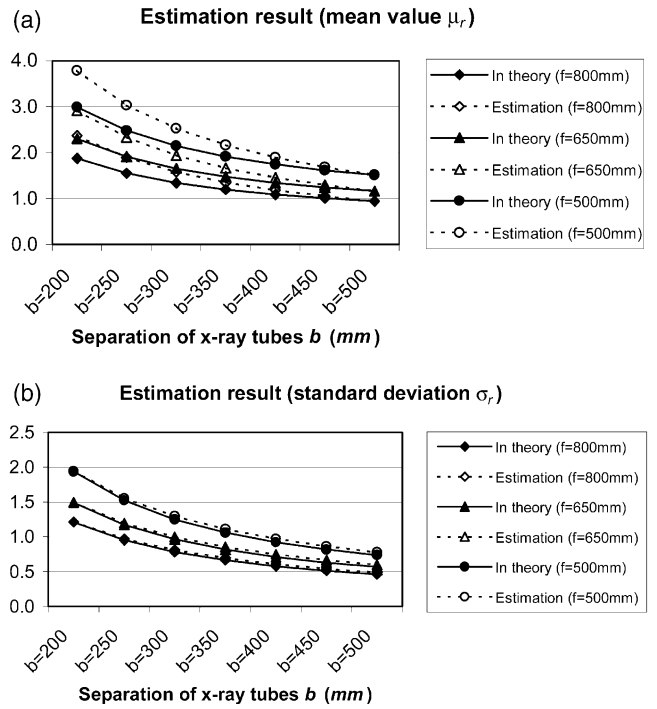


Fig. 7. Comparison between estimation results and numerical integration results. The object point was fixed, but system geometric parameters varied in this case.

gration formula (Eq. (7)). The formula was derived with probability theory, which provides a gold standard for calculating localization error. The formula, however, is not convenient in practice. We therefore derived an

approximation analytic formula (Eq. (10)), which can be used to make an acceptable estimation in system design and clinical practice.

The results of our analysis indicate that both the mean value and the standard deviation of the 3D localization error are inversely proportional to the source–image–distance f and the X-ray tubes separation b . The errors are proportional to parameter z (the distance from the object to the X-ray source), as summarized by Eq. (10). The results of our simulation experiments are in good agreement with the theoretical prediction.

Many factors affect the 3D localization accuracy. It is hard to balance the trade-off between different factors during stereo imaging in clinical practice. The mathematical formulas presented in this paper can be used as a practical guideline for such trade-off. For example, with our prototype system [13,14,21,22], when $f=600$ mm, $b=200$ mm and the biopsy needle-tip is located at $z=490$ mm, the 3D localization error of the needle-tip is quantified as a mean value of $\mu_r=2.5\sigma_m$, which means that the overall error is 2.5 times of the standard deviation of the measuring error. By increasing b from 200 to 500 mm, the mean value of 3D error is decreased to $\mu_r=1.30\sigma_m$ a 48% improvement in accuracy. But in clinical practice, the separation of the X-ray tubes may be limited to 300 mm, then the 3D localization error is $\mu_r=1.8\sigma_m$ in such case.

Eq. (12) gives another analytic means to express the 3D localization error. The analytic results clearly show that the mean value and the variance of 3D localization error are both inversely proportional to the magnification the X-ray system and the object view angle with the X-ray tubes, and are also both proportional to the variance of measuring errors as expected.

Acknowledgements

This research was supported in part by PHHS grants (CA69043 and CA70209; PI: Hong Liu) from National Institute of Health (NIH), a US Army breast cancer grant (DAMD 17-97-1-7138; PI: Hong Liu), grants (AP00(2)-011P and AP01(1)-016; PI: Wei R. Chen) from Oklahoma Center for Advancement of Science and Technology (OCAST), and by a grant from the University of Central Oklahoma (UCO; PI: Wei R. Chen). The authors would like to acknowledge the support of Charles and Jean Smith Chair endowment fund as well.

Appendix A

It is reasonable to assume that the errors, Δu_1 , Δu_2 , Δv_1 and Δv_2 of measurements are of similar characteristic, i.e. they have equal variance, say, σ_m^2 . With Gauss’s law of propagation of errors [23], it follows from Eq. (5) that

$$\begin{cases} \sigma_x^2 = \left[\left(\frac{\partial x}{\partial u_1} \right)^2 + \left(\frac{\partial x}{\partial u_2} \right)^2 + \left(\frac{\partial x}{\partial v_1} \right)^2 + \left(\frac{\partial x}{\partial v_2} \right)^2 \right] \sigma_m^2 \\ \sigma_y^2 = \left[\left(\frac{\partial y}{\partial u_1} \right)^2 + \left(\frac{\partial y}{\partial u_2} \right)^2 + \left(\frac{\partial y}{\partial v_1} \right)^2 + \left(\frac{\partial y}{\partial v_2} \right)^2 \right] \sigma_m^2 \\ \sigma_z^2 = \left[\left(\frac{\partial z}{\partial u_1} \right)^2 + \left(\frac{\partial z}{\partial u_2} \right)^2 + \left(\frac{\partial z}{\partial v_1} \right)^2 + \left(\frac{\partial z}{\partial v_2} \right)^2 \right] \sigma_m^2 \end{cases} \quad (A1)$$

Let:

$$\begin{cases} p(u_1, u_2) = (u_1 - u_2) + b \\ q(v_1, v_2) = (v_1 - v_2) \\ g(u_1, u_2) = (u_1 + u_2) / 2 \\ h(v_1, v_2) = (v_1 + v_2) / 2 \end{cases} \quad (A2)$$

Eq. (3) can be rewritten as:

$$\begin{cases} x = \frac{b \cdot p \cdot g}{p^2 + q^2} = \frac{z \cdot g}{f} \\ y = \frac{b \cdot p \cdot h}{p^2 + q^2} = \frac{z \cdot h}{f} \\ z = \frac{b \cdot p \cdot f}{p^2 + q^2} \end{cases} \quad (A3)$$

Using Eq. (A3)Eq. (A2), differentiate x , y and z with respect to u_1 , u_2 , v_1 and v_2 , respectively. Substituting the results into Eq. (A1) yields:

$$\begin{cases} \sigma_x^2 = \left\{ \frac{z^2}{2f^2} + \frac{2g^2b^2p^4}{(p^2+q^2)^4} \left(1 + \frac{q^4}{p^4} + \frac{4q^2p}{p^2} \right) + \frac{2zgbp^2}{f(p^2+q^2)^2} \left(\frac{q^2}{p^2} \right) \right\} \cdot \sigma_m^2 \\ \sigma_y^2 = \left\{ \frac{z^2}{2f^2} + \frac{2h^2b^2p^4}{(p^2+q^2)^4} \left(1 + \frac{q^4}{p^4} + \frac{4q^2}{p^2} \right) \right\} \cdot \sigma_m^2 \\ \sigma_z^2 = 2 \cdot \left(\frac{fbp}{(p^2+q^2)} \right)^2 \cdot \left(\frac{p}{(p^2+q^2)} \right)^2 \cdot \left(\frac{q^4}{p^4} + 1 + \frac{4q^2}{p^2} \right) \cdot \sigma_m^2 \end{cases} \quad (A4)$$

With the definition of q (see Fig. 2), the value of $q(v_1 - v_2)$ its value is very small in practice (in fact, it approaches zero in the noise-free case). So we have,

$$\left| \frac{q}{p} \right| = \frac{|v_1 - v_2|}{(u_1 - u_2) + b} \approx 0. \text{ Following Eq. (A3), we have:}$$

$$\begin{cases} \sigma_x^2 \approx \left(\frac{z^2}{2f^2} + \frac{2g^2b^2p^4}{(p^2+q^2)^4} \right) \cdot \sigma_m^2 = \frac{z^2}{2f^2} \left(1 + \frac{4x^2}{b^2} \right) \cdot \sigma_m^2 \\ \sigma_y^2 \approx \left(\frac{z^2}{2f^2} + \frac{2h^2b^2p^4}{(p^2+q^2)^4} \right) \cdot \sigma_m^2 = \frac{z^2}{2f^2} \left(1 + \frac{4y^2}{b^2} \right) \cdot \sigma_m^2 \\ \sigma_z^2 \approx \left(\frac{2f^2b^2p^4}{(p^2+q^2)^4} \right) \cdot \sigma_m^2 = \frac{2z^4}{f^2b^2} \cdot \sigma_m^2 \end{cases} \quad (A5)$$

This is Eq. (8) in Section 2.

We now solve the covariance between the components of localization error. The covariance between Δx , Δy and Δz can be derived using Eq. (5) [19]:

$$\begin{cases} \mu_{xy} = E[\Delta x \Delta y] = \left(\frac{\partial x}{\partial u_1} \frac{\partial y}{\partial u_1} + \frac{\partial x}{\partial u_2} \frac{\partial y}{\partial u_2} + \frac{\partial x}{\partial v_1} \frac{\partial y}{\partial v_1} + \frac{\partial x}{\partial v_2} \frac{\partial y}{\partial v_2} \right) \sigma_m^2 \\ \mu_{xz} = E[\Delta x \Delta z] = \left(\frac{\partial x}{\partial u_1} \frac{\partial z}{\partial u_1} + \frac{\partial x}{\partial u_2} \frac{\partial z}{\partial u_2} + \frac{\partial x}{\partial v_1} \frac{\partial z}{\partial v_1} + \frac{\partial x}{\partial v_2} \frac{\partial z}{\partial v_2} \right) \sigma_m^2 \\ \mu_{yz} = E[\Delta y \Delta z] = \left(\frac{\partial y}{\partial u_1} \frac{\partial z}{\partial u_1} + \frac{\partial y}{\partial u_2} \frac{\partial z}{\partial u_2} + \frac{\partial y}{\partial v_1} \frac{\partial z}{\partial v_1} + \frac{\partial y}{\partial v_2} \frac{\partial z}{\partial v_2} \right) \sigma_m^2 \end{cases} \quad (A6)$$

Similar to the variance estimation procedure, with Eq. (A3) and Eq. (A2), take partial derivatives with respect to u_1 , u_2 , v_1 and v_2 , respectively. Substituting the results into Eq. (A6) and noticing the fact that $|q/p| \approx 0$, we have:

$$\begin{cases} \mu_{xy} = \frac{2xyz^2}{b^2f^2} \sigma_m^2 \\ \mu_{xz} = \frac{2xzz^2}{b^2f^2} \sigma_m^2 \\ \mu_{yz} = \frac{2yzz^2}{b^2f^2} \sigma_m^2 \end{cases} \quad (A7)$$

This is Eq. (9) in Section 2.

References

- [1] Fajardo L, Willison K, Pizzutiello R. A comprehensive approach to stereotactic breast biopsy. Boston, MA: Blackwell Science Inc, 1996.
- [2] Alexander III E, Loeffler J, Lunsford L. Stereotactic radiosurgery. New York: McGraw-Hill, 1993.
- [3] Barnett G, Roberts D, Maciunas R. Image-guided neurosurgery. St Louis, MI: Quality Medical Publishers, 1998.
- [4] Gildenburg P, Tasker R. Textbook of stereotactic and functional microsurgery. New York: McGraw-Hill, 1998.
- [5] Longuet-Higgins H. A computer algorithm for reconstructing a scene from two projections. *Nature* 1981;293:133–5.
- [6] Mayhew J, Longuet-Higgins H. A computation model for binocular depth perception. *Nature* 1982;297:376–8.
- [7] Fagueras O. Three-dimensional computer vision. Cambridge, MA: MIT Press, 1993.
- [8] Metz C, Fencil L. Determination of three-dimensional structure in biplane radiography without prior knowledge of the relationship between the two views: theory. *Medical Physics* 1989;16:45–51.
- [9] Fencil L, Metz C. Propagation and reduction of error in three-dimensional structure determined from biplane views of unknown orientation. *Medical Physics* 1990;17:951–61.
- [10] Hoffmann K, Metz C, Chen Y. Determination of 3D imaging geometry and object configurations from two biplane views: an enhancement of the Metz–Fencil technique. *Medical Physics* 1995;22:1219–27.
- [11] Chen S, Metz C. Improved determination of biplane imaging geometry from two projection images and its application to three-dimensional reconstruction of coronary arterial trees. *Medical Physics* 1997;24:633–54.
- [12] Ganapathy S. Decomposition of transformation matrices for robot vision. *Pattern Recognition Letters* 1984;2:401–12.
- [13] Jiang H, Liu H, Fajardo L. Positional accuracy and sensitivity in X-ray stereo-image guidance. *SPIE Proceedings* 1999;3595:178–85.
- [14] Jiang H, Liu H, Wang G, Chen W, Fajardo L. A localization algorithm and error analysis for stereo X-ray image guidance. *Medical Physics* 2000;27:885–93.
- [15] Rade L, Westergren B. Mathematics handbook for science and engineering. Cambridge, MA: Birkhauser, 1995.
- [16] Press W, Teukolsky B, Vetterling W, Flannery B. Numerical recipes. 2nd ed. Cambridge: Cambridge University Press, 1992.
- [17] Hill RO Jr. Elementary linear algebra with applications. 3rd ed. Philadelphia: Saunders College Publishers, 1996.
- [18] Hsu DY. Spatial error analysis. Piscataway, NJ: IEEE Press, 1999.
- [19] Papoulis A. Probability, random variables, and stochastic processes. 3rd ed. Boston, MA: McGraw-Hill, 1991.
- [20] Curry III T, Dowdey J, Murry R Jr. Introduction to the physics of diagnostic radiology. 3rd ed. Philadelphia, PA: Lea and Febiger, 1984.
- [21] Liu H, Fajardo L, Penny B. Signal-to-noise ratio, noise power spectrum and detective quantum efficiency analysis of optically coupled CCD mammography imaging systems. *Academic Radiology* 1996;3:799–805.
- [22] Liu H, Xu J, Halama G, McAdoo J. Digital fluoroscopy using an optically coupled CCD: Preliminary investigations. *SPIE Proceedings* 1997;2976:256–61.
- [23] Gellert W, Gottwald S et al. The VNR concise encyclopedia of mathematics. 2nd ed. New York: Van Nostrand Reinhold, 1989.